ELSEVIER

0144-8617(94)00067-0

Carbohydrate Polymers **25** (1994) 319–329
Elsevier Science Limited.
Printed in Great Britain
0144-8617/94/$07.00 + .00

Predicting the rheology of food biopolymers using constitutive models

J. L. Kokini

Center for Advanced Food Technology, Department of Food Science, Rutgers, The State University of New Jersey, PO Box 231, New Brunswick, NJ 08903-0231, USA

(Received 30 March 1994; revised version received 30 August 1994; accepted 1 September 1994)

Several constitutive models have been discussed to explain data for some foods in diluted and concentrated systems. Firstly, the theories of Rouse and Zimm, as well as rod-like theory, were used to study the conformation of the pectins in dilute solution. Among the dilute theories, the random coil theory of Zimm best explained the experimental data and suggested a certain level of intermolecular interaction present in the dilute pectin solution.

The Bird–Carreau constitutive theory with four empirical constants and zero shear limiting viscosity was used to describe the viscoelastic properties of the solutions of the guar, CMC/guar, glutenin, gluten and wheat flour doughs. The Bird–Carreau model was able to predict η and η' in the high and low frequency regions for 1% guar solution. In the case of CMC/guar blend, the Bird–Carreau model explained steady shear and dynamic properties very well in the higher shear rate or frequency region of 1–100 s^{-1}. However, η''/ω does not tend to a zero shear constant value. The Bird–Carreau model also gave good predictions on the rheological properties of gluten and glutenin biopolymers in the free-flow region.

The polydisperse type, Doi–Edwards model, fits the experimental G' and G'' better than the monodisperse model for 5% apple pectin dispersion. However, there is still a discrepancy between experimental and predicted values.

INTRODUCTION

Constitutive models aim at relating rheological properties to molecular architecture and to prediction of all components of stress generated as a result of a given deformation history. In order to achieve this goal idealizations of molecular architecture or conformation are necessary. Such idealizations lead to molecular theories of rheology. A typical idealization is the use of the freely jointed chain consisting of springs and beads (Bird *et al.*, 1987; Bagley, 1992; Darby, 1976). Molecular theories' evolution started by considering dilute solutions of high molecular weight polymeric materials. These theories are particularly useful in characterizing the effect of long range conformation on flexibility of carbohydrates as well as proteins. The theories of Rouse (1953) and Zimm (1956) are applicable to polymers with a random coil configuration, while those of Marvin and McKinney (1965) predict rod-like conformations.

Dilute solution molecular theories have evolved to also predict rheological properties of concentrated polymeric systems. Some constitutive theories are based on principles of continuum mechanics such as the Bird–Carreau model (1968) and are semi-empirical in nature. Such models incorporate key assumptions pertaining to network formation and dissolution which clearly occur during deformation processes. The semi-empiricism facilitates the estimation of parameters and makes the models easily applicable to a variety of materials such as concentrated dispersions of polysaccharides (Kokini & Plutchok, 1987), protein networks as well as doughs (Dus & Kokini, 1990; Cocero & Kokini, 1991.

Other constitutive models have an accurate molecular and conformational basis and enable us to predict rheological properties from detailed understanding of molecular structure. An example is Doi–Edwards constitutive model (Doi & Edwards, 1978*a*, *b*, *c*). While these models do not currently permit prediction of the rheological properties of complex mixtures, they nevertheless provide major clues in designing food molecules with desired rheological properties.

The objective of this review is to discuss some of the constitutive models described above and to present data for some food systems.

DILUTE SOLUTION MOLECULAR THEORIES

The equations to predict the reduced moduli and relaxation time of flexible random coil molecules of Rouse and Zimm type are as follows:

$$[G']_R = \sum_{p=1}^{n} \frac{\omega^2 \tau_p^2}{(1 + \omega^2 \tau_p^2)}. \quad (1)$$

Table 1 shows the values of these constants for five different rigid-rod models. The predicted reduced moduli from the theory of Marvin and McKinney (1965) for rigid dumb-bells as a function of $\omega\tau$ are given in Fig. 1 and those for the random coil theories of Rouse and Zimm are shown in Fig. 2. At high frequencies the reduced moduli of the Rouse theory become equal and increase together with a slope of 1/2, while those in the Zimm theory remain unequal and increase in a parallel manner with a slope of 2/3.

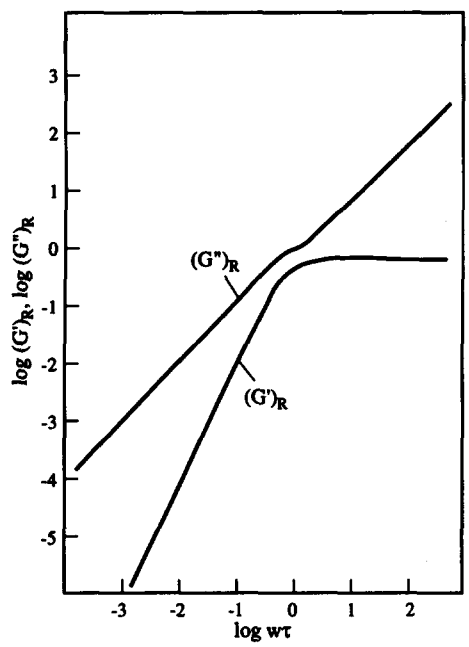

Fig. 1. Variation of reduced modulus with $\omega\tau$ for rigid rods.

Table 1. Empirical constants m_1 and m_2 for the elongated rigid rod model

Model	m_1	m_2	m
Cylinder	0.60	0.29	1.15
Cylinder	0.46	0.16	1.61
Rigid dumbell (Marvin & McKinney, 1965)	0.60	0.40	1.00
Prolate ellipsoid	0.60	0.24	1.19
Shishkebob	0.60	0.20	1.25

CONCENTRATED SOLUTION/MELT THEORIES

The Bird–Carreau model

This model involves taking an integral over the entire deformation history of the material (Bistany & Kokini, 1983). James (1947) was first to develop a mathematical model for statistical properties of a molecular network (Plutchok & Kokini, 1986) which consists of physically crosslinked polymer chains, forming a macromolecular structure. The Bird–Carreau model is based on the Carreau constitutive theory of molecular networks which is able to explain viscoelastic behavior by assuming that deformation creates and destroys temporary crosslinks (Leppard, 1975).

The model uses four empirical constants and the zero shear limiting viscosity of the solutions. The constants, α_1 and λ_1 are obtained from a logarithmic plot of η vs γ and the other two constants α_2 and λ_2 are obtained from a logarithmic plot of η vs ω as shown in Fig. 3.

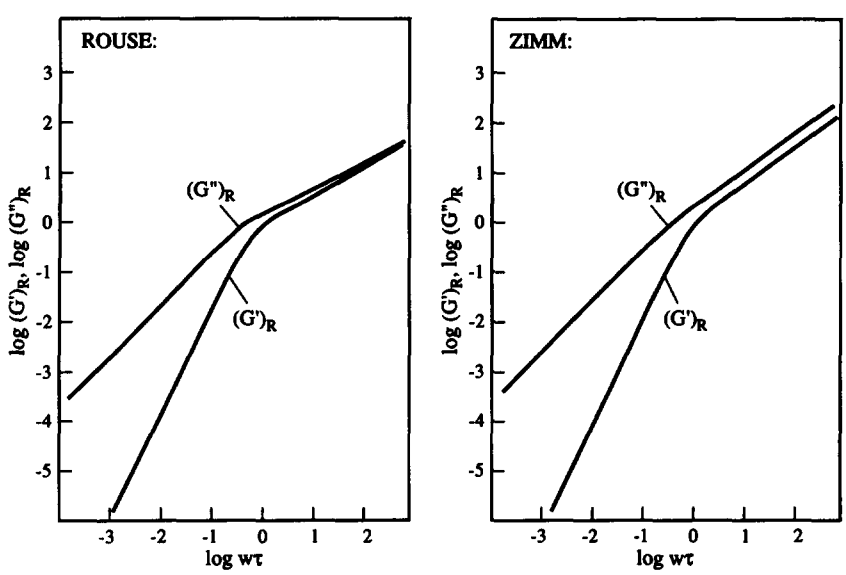

Fig. 2. Variation of reduced modulus with $\omega\tau$ for random coils.

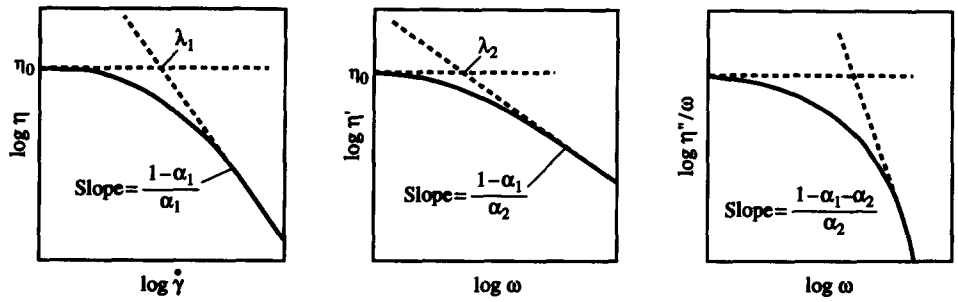

Fig. 3. Viscosity vs shear rate plots leading to empirical constants for the Bird–Carreau model.

The prediction for η is:

$$\eta = \sum_{p=1}^{\infty} \frac{np}{1 + (\lambda_1 p\dot{\gamma})^2} \quad \text{and} \tag{2}$$

$$\eta = \frac{\pi\eta_0}{z(\alpha_1) - 1} \cdot \frac{(2^{\alpha}1\lambda_1\dot{\gamma})^{(1-\alpha)/\alpha_1}}{z(\alpha_1 \sin\left[\dfrac{1-\alpha_1}{2\alpha_1} \cdot \pi\right]} \quad \text{at large shear rates,} \tag{3}$$

where

$$\lambda_{1p} = \lambda_1 \left[\frac{2}{p+1}\right]^{\alpha_1} \tag{4}$$

$$\eta_p = \eta_0 \frac{\lambda_{1p}}{\sum_{p=1}^{\infty} \lambda_{1p}} \tag{5}$$

$$z(\alpha_1) = \sum_{k=1}^{\infty} K^{-\alpha_1}. \tag{6}$$

The prediction of η' is:

$$\eta' = \sum_{p=1}^{\infty} \frac{\eta p}{1 + (\lambda_{2p}\omega)^2} \tag{7}$$

and

$$\eta' = \frac{\pi\eta_0}{z(\alpha_1) - 1} \cdot \frac{(2\alpha_2\lambda_2\omega)^{(1-\alpha_1)/\alpha_2}}{2\alpha_2 \sin\left[\dfrac{1 + 2\alpha_2 - \alpha_1}{2\alpha_2} \cdot \pi\right]}$$

at high frequencies. (8)

The Bird–Carreau model for η''/ω is:

$$\eta''/\omega = \sum_{p=1}^{\infty} \frac{\eta_p\lambda_{2p}}{1 + (\lambda_{2p}\omega)^2} \quad \text{and} \tag{9}$$

$$\eta''/\omega = \frac{2^{\alpha_2}\lambda_2\pi\eta_0}{z(\alpha_1) - 1} \cdot \frac{(2^{\alpha_2}\lambda_2\omega)^{(1-\alpha_1-\alpha_2)/\alpha_2}}{2\alpha_2 \sin\left[\dfrac{1 + \alpha_2 - \alpha_1}{2\alpha_2} \cdot \pi\right]}$$

at high frequency, (10)

where

$$\lambda_{2p} = \lambda_2 \left[\frac{2}{p+1}\right]^{\alpha_2}. \tag{11}$$

The Doi–Edwards model

In the Doi–Edwards theory (Doi & Edwards, 1978*a*,*b*,*c*), viscoelasticity is explained by considering entanglements within the polymer network. Accordingly, a model chain (or primitive path) is constructed which describes molecular motions in a densely populated system using appropriate assumptions. For example, each polymer chain moves independently in the mean field imposed by the other chains. The mean field is represented by a three-dimensional cage. In this cage each polymer is confined in a tube-like region surrounding it as shown in Fig. 4. The primitive chain can move randomly forward or backward only along itself.

To define dynamic properties under flow, a sliplink network concept is introduced. The junctions of sliplinks are assumed not to be permanent crosslinks but small rings through which the chain can pass freely. This gives a simple molecular mechanism for the breakage and creation process as it occurs by the sliding motion of the chain through the sliplinks as shown in Fig. 5. In a system of highly entangled polymers, the molecular motion of a single chain can be divided into two types: (i) the small scale wiggling motion which does not alter the topology of the entanglement; and (ii) the large scale diffusive motion which changes the topology.

The time scale of the first motion is essentially the Rouse relaxation time (Shrimanker, 1989). The time

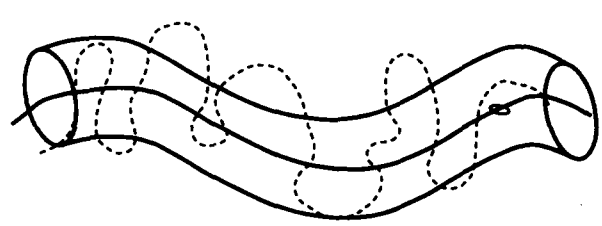

Fig. 4. A schematic representation of a worm-like polymer chain (dashed line) surrounded by an outer tube-like cage.

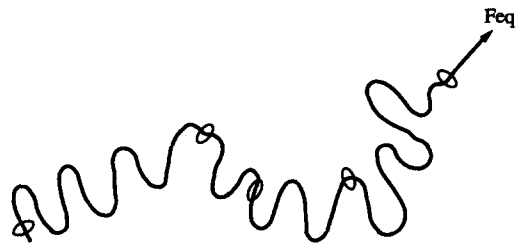

Fig. 5. A schematic representation of the sliding motion of the wiggling chain through sliplinks (small circles).

scale of the second motion denoted by T_d is a renewal proportion of the topology of a single chain and is proportional to M^3 (Doi & Edwards, 1978*a*,*b*,*c*). The Doi–Edwards theory is only concerned with motion of the second type. For a polydisperse system, the theory has been modified by Rahalkar *et al.* (1985). The following results are relevant to the storage and loss moduli (G' and G'') of a monodisperse polymer.

$$G'(\omega) = \frac{8}{\pi^2} G^0 N \sum_{p=1,\text{odd}}^{\infty} [(\omega T_1)^2/p^6]/[1 + (\omega T_1)^2/p^4] \tag{12}$$

$$G''(\omega) = \frac{8}{\pi^2} G^0 N \sum_{p=1,\text{odd}}^{\infty} [(\omega T_1)/p^6]/[1 + (\omega T_1)^2/p^4], \tag{13}$$

where G_N^0 is the plateau modulus obtained at high frequency, p is an integer.

For a polydisperse polymer with a molecular weight distribution $f(\mu)$, the weight fraction of chains with molecular weight between M and $M + dM$ is given by $W(M)\,dM$ where

$$W(M) = 1/M_n f(\mu), \tag{14}$$

where μ is the dimensionless molecular weight ($=M/M_n$).

For this case, the storage and loss modulus are given by:

$$G'(\omega) = G_N^0 \int_0^{\infty} 8/\pi^2 \sum_{p=1,\text{odd}}^{\infty} [(\omega T_1)^2 \mu^6 f(\mu)/p^6]/$$

$$[1 + (\omega T_1)^2 \mu^6/p^4] d\mu \tag{15}$$

and

$$G''(\omega) = G_N^0 \int_0^{\infty} 8/\pi^2 \sum_{p=1,\text{odd}}^{\infty} [(\omega T_1)\mu^3 f(\mu)/p^4]/$$

$$[1 + (\omega T_1)^2 \mu^6/p^4] d\mu, \tag{16}$$

where G_N^0, the plateau modulus is given by

$$G_N^0 = G_0 \text{ave}/5. \tag{17}$$

APPLICATIONS OF CONSTITUTIVE MODELS TO FOOD SYSTEMS

Dilute solution theories

We used the theories of Rouse and Zimm as well as rod-like theories to study the conformation of apple, tomato and citrus pectins in solution. Estimation of intrinsic moduli $[G']$ and $[G'']$ necessitates measurement of the storage modulus G' and the loss modulus G'' at several concentrations in the dilute solution region and then extrapolation to zero concentration. Small amplitude oscillatory measurements were conducted in 0.25 M NaCl to achieve maximum dissociation between chains, in 95% glycerol/5% deionized water mixtures as solvent.

The reduced moduli were then calculated from intrinsic moduli by taking molecular weights and temperature into account. The longest relaxation time was calculated by using the Rouse approximation:

$$\tau = \frac{6[\eta]\eta_s M}{\pi^2 RT} \tag{18}$$

where $[\eta]$ is the intrinsic viscosity, η_s is the solvent viscosity, M is the molecular weight and T is the absolute temperature.

The fit of the experimental reduced moduli $[G']_R$ and $[G'']_R$ with the theoretical rigid rod model of Marvin and McKinney (1965) for apple pectin of degree of methylation 73.5% is shown in Fig. 6. It indicates that this material does not follow rod-like behavior. Experimental reduced moduli are also compared with predictions of the Rouse and Zimm models (Figs 6–8). The fit

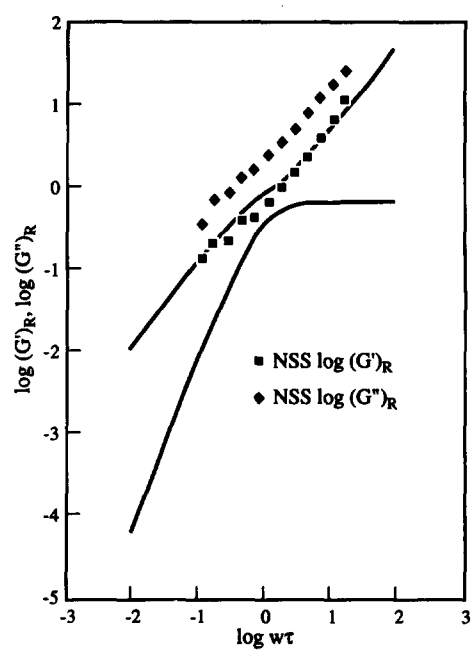

Fig. 6. Comparison of experimental reduced moduli of NSS (upper curve) with rod model (lower curve).

is better than that in the rod-like model, but nevertheless the data are not well approximated by this theory either. Similar comparison of the experimental reduced moduli with the predictions of the theoretical random coil theory of Zimm can be seen in Fig. 8 for 73.5% pectin. Here, the data follow the expected values for Zimm type behavior relatively well with the limiting slope of the reduced moduli closer to the calculated slopes of 2/3 for the Zimm model than that of 1/2 for the Rouse model. This suggests a certain level of intermolecular interaction. This interaction is expected since like charges on the molecule will tend to repel, while opposite charges attract.

Concentrated systems

The Bird–Carreau model has been tested with a wide variety of food materials including guar and carrageenan gums, carboxymethyl cellulose, high moisture wheat gluten and wheat glutenin: hard and soft wheat flour as well as mixtures of guar gum and sodium carboxymethylcellulose. The following discussion will present data for some of these materials.

APPLICATION OF THE BIRD–CARREAU MODEL TO CONCENTRATED GUM DISPERSIONS

Solutions of polysaccharides in the concentration range of value to the food industry have been shown to be non-Newtonian in steady shear flows at large enough shear rates (Schurz, 1976; Glicksman, 1982). In transient flows, such as small amplitude oscillatory shear flows, they show both elasticity and viscosity and their viscoelasticities are linear at small strains.

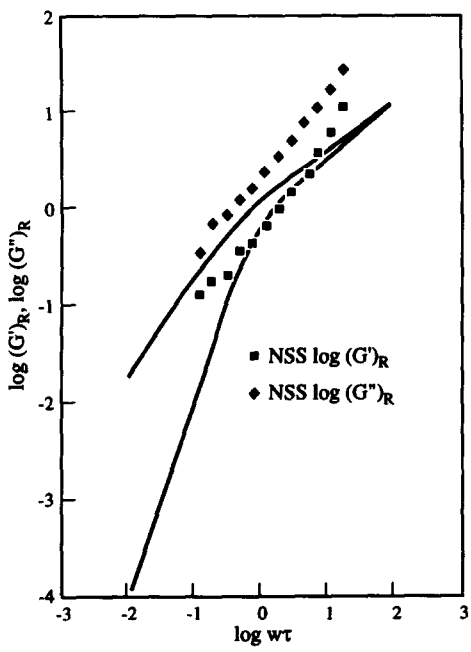

Fig. 7. Comparison of experimental reduced moduli of NSS (upper curve) with Rouse model (lower curve).

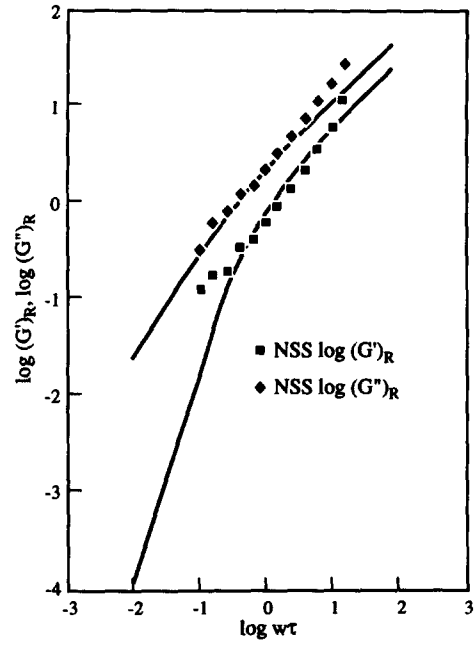

Fig. 8. Comparison of experimental reduced moduli of NSS (upper curve) with Zimm model (lower curve).

Rheological modeling is ideal when a single model can explain data obtained in several kinds of experiments. The data from one can then be used to predict what the data would be from another experiment. The Bird–Carreau model is able to satisfy this need.

The empirical constants η_0, λ_1, λ_2, α_1 and α_2 for 1 and 1.25% guar carrageenan and CMC dispersions are given in Table 2.

In Fig. 9, predictions using the Bird–Carreau model are compared with experimental data for 1.0% guar solution in the frequency/shear rate range of 0.1–100 s^{-1}. For η''/ω, the model very accurately predicted the high frequency region, the coefficient of determination (R^2) in this region was 0.99. The low frequency regions were somewhat less accurately predicted, the R^2 in this region being 0.97. This could be due to the fact that parameters λ_1, λ_2, α_1 and α_2 were determined using the procedure of Bird *et al.* (1977). This procedure was selected because of its simplicity. An alternative procedure could be used to curve-fit the η vs $\dot{\gamma}$ and η vs ω data to obtain the four parameters. Similarly, experimental values of η' vs ω and η vs $\dot{\gamma}$ were fitted quite accurately by the model as demonstrated by R^2 values of 0.99 and 0.98, respectively, in the high and low frequency regions.

BLENDS OF CMC AND GUAR GUM

Owing to functionality and cost consideration, blends of food gums are often used in food formulations; therefore, the ability to predict steady and oscillatory rheo-

Table 2. Bird–Carreau parameters for guar, carrageenan and CMC gums

		η_0	α_1	α_2	λ_1 (s)	λ_2 (s)
Guar	0.5%	2.00	1.62	1.04	0.21	0.40
	0.75%	12.62	2.12	1.53	0.42	0.87
Guar	1%	20.0	3.33	3.19	1.33	2.50
	1.25%	70.0	5.85	5.67	1.56	3.57
Carrageenan	2.0%	4.8	1.88	1.81	0.426	0.444
	2.5%	13.5	2.43	2.24	0.585	0.763
CMC	0.50%	0.99	1.27	0.01	0.12	0.21
	0.75%	2.60	1.33	1.02	0.26	0.22
	1.00%	7.61	1.45	1.05	0.36	0.33
	1.50%	28.94	1.60	1.30	0.77	1.54

logical properties of blends of gums from component properties becomes a significant capability.

A generalized correlation to predict rheological constants from concentration and molecular weight of the following form was used:

$$f(c_{\text{blend}}, \bar{M}_{w,\text{blend}}) = p_0(c_{\text{blend}})p_1(\bar{M}_{w,\text{blend}})p_2, \tag{19}$$

where

p_0, p_1, p_2 = parameters to be determined;
c = concentration (g/100 ml);
M_w = weight-average molecular weight;
$f(c_{\text{blend}}, \bar{M}_{w,\text{blend}}) = \eta_0, \lambda_1, \lambda_2, s_\eta, s_\eta'$;
$s_\eta = -\text{slope}_\eta$; and $s_\eta' = -\text{slope}_\eta'$;

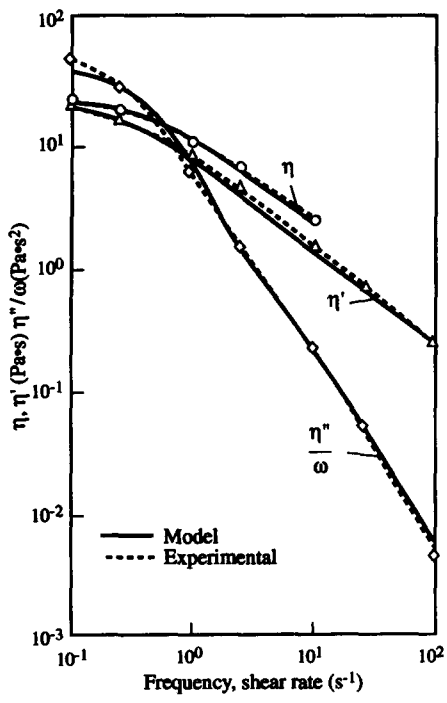

Fig. 9. Predictions of the Bird–Carreau model for 1.0% guar: solid lines represent experimental data and dotted lines represent predictions of the Bird–Carreau model.

and

$\bar{M}_{w,\text{blend}} = X_1\bar{M}_{w,1} + X_2\bar{M}_{w,2}, X_i$ = mass fraction;
$c_{\text{blend}} = v_1c_1 + v_2c_2, v_i$ = volume fraction.

The least squares estimators of best fit p_0, p_1, p_2 were determined for experimental values of $\eta_0, \lambda_1, \lambda_2, s_\eta$ and $s_{\eta'}$ and substituted into eqn (19) to calculate the predicted values of $\eta_0, \lambda_1, \lambda_2, \alpha_1$ and α_2 (Table 3). Plots of experimental vs predicted values of η_0 and λ_1 are presented in Fig. 10 as an example. Values for η_0 are plotted on log-log coordinates to accommodate the range of magnitudes.

Regression analysis of the experimental data with concentration (c) and $\bar{M}_w$ data resulted in an empirical equation capable of predicting each material constant. These equations are as follows for CMC, guar gum and CMC/guar blends of ratios 3:1, 2:1, 1:1, 1:2 and 1:3 by weight in the concentration range of 0.5–1.5% by weight:

$$\eta_p = 1.06 \times 10^{19}(C_{\text{blend}})^{3.63}(\bar{M}_{w,\text{blend}})^{-2.94} \tag{20}$$

$$\lambda_1 = 1.81 \times 10^{5}(C_{\text{blend}})^{1.75}(\bar{M}_{w,\text{blend}})^{-0.92} \tag{21}$$

$$\lambda_2 = 1.63 \times 10^{9}(C_{\text{blend}})^{1.72}(\bar{M}_{w,\text{blend}})^{-1.72} \tag{22}$$

$$s_\eta = 1.63 \times 10^{7}(C_{\text{blend}})^{0.50}(\bar{M}_{w,\text{blend}})^{-1.26} \tag{23}$$

Table 3. Bird–Carreau constants predicted from c_{blend} and M_w, blend

Material[a]	Conc (%)	η_0 (poise)	λ_1 (s)	λ_2 (s)	α_1	α_2
CMC	0.50	0.91	0.13	0.20	1.31	0.92
	0.75	3.96	0.26	0.40	1.41	1.07
	1.00	11.24	0.43	0.66	1.50	1.20
	1.50	48.93	0.88	1.33	1.70	1.46
3:1	0.50	1.24	0.14	0.24	1.37	0.97
	0.75	5.41	0.29	0.48	1.50	1.14
	1.00	15.35	0.48	0.78	1.62	1.30
	1.50	66.84	0.97	1.56	1.88	1.63
2:1	0.50	1.39	0.15	0.25	1.40	0.98
	0.75	6.05	0.30	0.50	1.53	1.61
	1.00	17.17	0.49	0.83	1.67	1.34
	1.50	74.75	1.01	1.66	1.97	1.70
1:1	0.50	1.76	0.16	0.28	1.46	1.03
	0.75	7.67	0.32	0.57	1.63	1.23
	1.00	21.76	0.53	0.94	1.80	1.44
	1.50	94.77	1.08	1.88	2.20	1.89
1:2	0.50	2.28	0.17	0.33	1.54	1.08
	0.75	9.93	0.35	0.65	1.75	1.33
	1.00	28.18	0.58	1.07	1.99	1.59
	1.50	122.71	1.18	2.15	2.55	2.20
1:3	0.50	2.62	0.18	0.35	1.59	1.12
	0.75	11.40	0.36	0.70	1.84	1.39
	1.00	32.36	0.60	1.15	2.11	1.69
	1.50	140.91	1.23	2.31	2.82	2.43
Guar	0.50	4.14	0.21	0.45	1.83	1.28
	0.75	18.03	0.42	0.89	2.25	1.70
	1.00	51.18	0.70	1.46	2.79	2.22
	1.50	222.85	1.42	2.93	4.66	4.01

[a] Blends are CMC/guar.

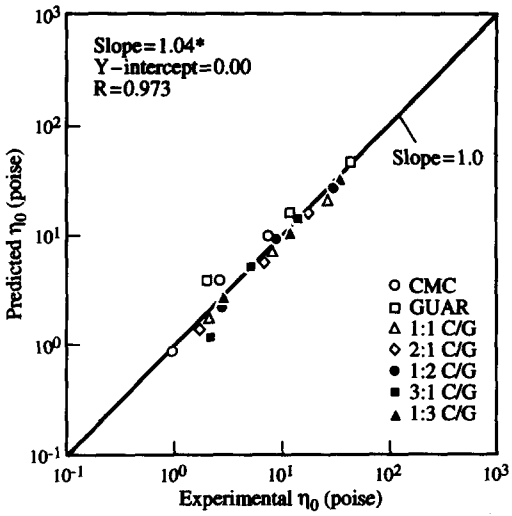

Fig. 10. Experimental η_0 vs predicted η_0 for CMC/guar blend.

$$s_{\eta'} = 2.17 \times 7^{19}(C_{\text{blend}})^{0.32}(\bar{M}_{\text{w. blend}})^{-1.26}. \quad (24)$$

The Bird–Carreau predictions of η, η' and η''/ω are presented in Fig. 11 for 1.0% 3:1 CMC/guar blend as an example. Experimental data are superimposed on these plots to judge the aptness of the model. The steady shear viscosity η and the dynamic viscosity η' are extremely well predicted in the shear rate range of 0.1–100 s^{-1}. The experimental data as well as the theoretical predictions portray commonly observed behavior by polymeric dispersions. In this instance, η is larger than η' and the model predicts precisely that. η and η' for this blend ratio tend to the same value, a property suggested by the Bird–Carreau model at low shear rates (Kokini *et al.*, 1984)

On the other hand, η''/ω deviates from the experimental data. The data do not seem to tend to a zero shear constant value. The Bird–Carreau prediction, however, does tend to a zero shear constant value. This results in the ability of the prediction to succeed only in the frequency range of 1–100 s^{-1}. However, the discrepancy between the experimental data and the theoretical model widens as the shear rate tends to zero. In this case, the smallest shear rate where measurements could be made was 10^{-2} s^{-1}.

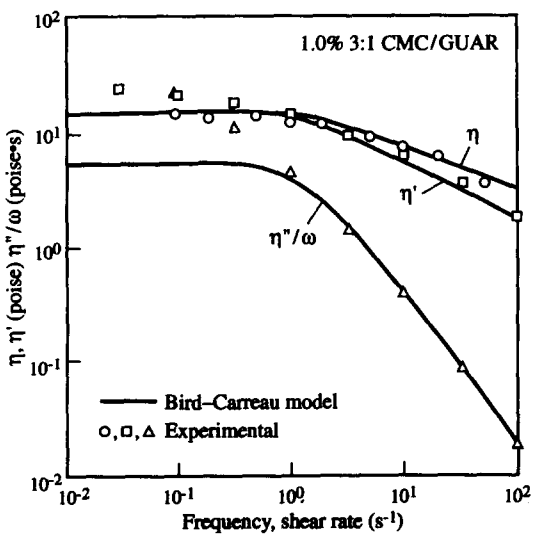

Fig. 11. Predictions of the Bird–Carreau model based on concentration and molecular weight for 1.0% 3:1 CMC/guar blend.

SIMULATION OF WHEAT GLUTENIN AND GLUTEN RHEOLOGICAL PROPERTIES

In the case of cereal biopolymers the rheological properties at moderate to low moisture content are highly significant. Proteins exist in any amorphous metastable glassy state which is very sensitive to changes in moisture, temperature and processing history.

Water acts as a plasticizer of the amorphous regions and depresses the glass transition temperature. Hoseney *et al.* (1986) and Cocero and Kokini (1991) showed that both gluten and its high molecular weight component glutenin were glassy, amorphous and plasticizable polymers with water acting as a plasticizer to depress gluten's glass transition temperature.

At temperatures below the glass transition (glassy state), the apparent viscosity is successfully predicted by the Arrhenius equation. At temperatures above the glass transition (typically from T_g to $T_g + 100°C$), in the rubbery range, the dependence of viscoelastic properties on temperature is successfully predicted by the Williams *et al.* (1955) equation. Each of these regions has implications in terms of dough processing. During extrusion, dough is expected to form and flow freely while after extrusion it is expected to be in the glassy region to generate a crisp texture. Similarly, during sheeting, dough needs to be viscoelastic to be shaped and formed adequately. After baking, many baked products need to be crispy and crunchy which requires that the material be in the glassy state.

Prediction of rheological properties is a key issue for product and process design. In the 'free-flow' regions, where the material flows, the Bird–Carreau model should be able to predict the rheology of both gluten and glutenin.

The glass transition line in the state diagram for glutenin was obtained from experiments conducted in the moisture range of 0–28%w, with T_g ranging between 141.9 and −71.7°C. The moisture and temperature above this line correspond to the rubbery domain. The Gordon and Taylor (1952) equation was fitted to the glass transition state to give a K value of 6.62 in Fig. 12. From the annealing experiments, the 'maximum concentrated solution (T_g') region' was obtained. This horizontal line in Fig. 12 depicts the region in the state diagram where ice and rubber co-exist.

When the time–temperature superposition principle was applied for the 40%w glutenin using 25°C as the

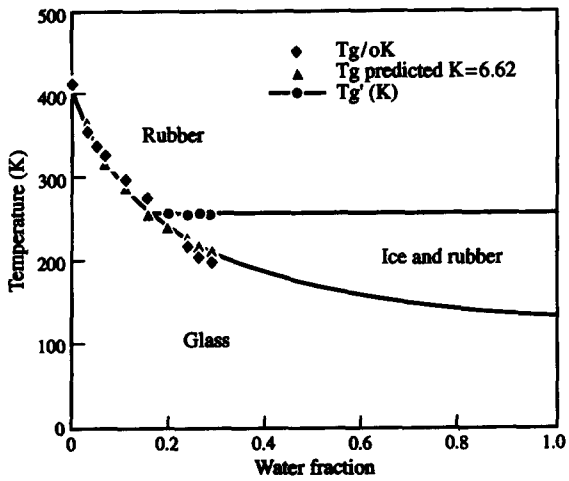

Fig. 12. Gordon and Taylor's fit for the glass transition in wheat glutenin state diagram.

reference temperature, the data were nicely superimposed to obtain the high shear rate viscosity data shown in Fig. 13. The shift factor (A_t) temperature dependence or the temperature dependence of the apparent viscosity for 40%w glutenin was better predicted by the Arrhenius equation, suggesting that we are in the domain of moisture and temperature where the material flows. The low shear rate viscosity data obtained using the mechanical spectrometer (Rheometrics RMS-800) and Rheometrics stress rheometer (RSR) superimposed very nicely with the viscosity data obtained from the capillary rheometer (Instron) providing steady viscosity data ranging from 10^{-6} to 10^{5} s^{-1}.

The Bird–Carreau equation successfully predicted the apparent steady shear viscosity for 40% moisture glutenin at 25°C. The Bird–Carreau parameters, zero-shear viscosity η_0, α_1 and λ_1 were obtained from the master or composite curve with values of 1.52×10^9 poise, 2.628 poise s, 1×10^5 s, respectively. These results suggest that this material is indeed in the 'free-flow region' of its state diagram. Since glutenin is the principal protein component of wheat flour dough, the presence of disulfide bonds and noncovalent interactions determine the density of entanglements. The dough experiences rubbery flow where the entanglements slip so that configurational rearrangements of segments separated by entanglements can take place (Ferry, 1980).

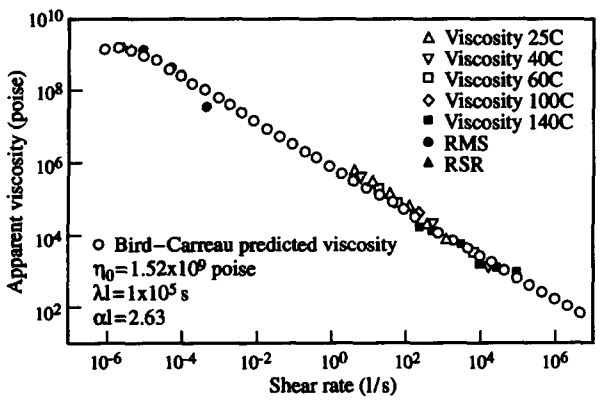

Fig. 13. Bird–Carreau prediction of the steady viscosity for 40% moisture glutenin at 25°C.

Steady viscosity data for gluten with 52.5% moisture, obtained from RMS, capillary rheometer and stress rheometer, are shown in Fig. 14 as another example. Three parameters of the Bird–Carreau model, zero shear viscosities (η_0), α_1 and λ_1, of 52.5%, 55% and 57.5% moisture gluten doughs are listed in Table 4. The result shows that these three parameters are moisture content dependent, the higher the moisture content the larger η_0 and λ_1 and the smaller α_1. Values of α_1 for 55% moisture gluten dough are similar to those for 57.5% moisture, but smaller than those for 52.5% moisture. α_2 values of 52.5%, 55% and 57.5% moisture doughs show the same dependence on moisture content as α_1. The values of λ_1 are much smaller than the values of λ_2 in all gluten doughs with different moisture content which implies that the gluten forms a network more easily than destroying a network. Using these parameters in the Bird–Carreau model gives excellent prediction for steady viscosity, η' and η''/ω for all three moisture gluten doughs and the R^2s are larger than 0.99; an example is given in Fig. 15.

Table 4. Parameters using Bird–Carreau model for predicting the rheological properties of gluten doughs with different moisture contents

Moisture (%)	η_0 (poise)	λ_1 (s)	α_1	α_2	λ_2 (s)
52.5	1.447×10^7	705	3.11847	3.34809	284000
55	1.318×10^7	625	3.43985	3.46030	81700
57.5	1.097×10^7	405	3.50869	3.52602	77700

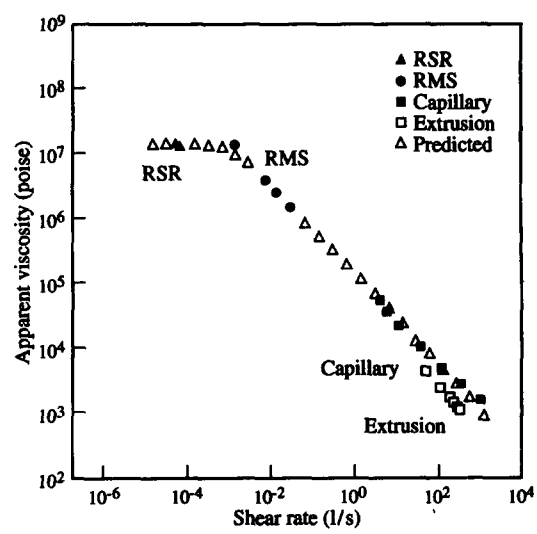

Fig. 14. Bird–Carreau prediction of the steady viscosity for 52.5% moisture gluten dough at 25°C.

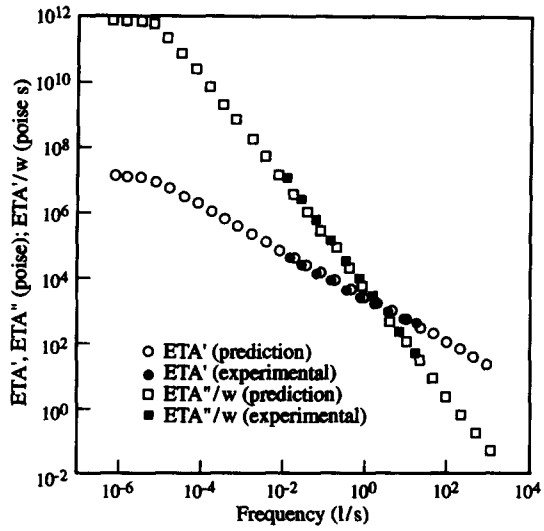

Fig. 15. Bird–Carreau prediction of η' and η''/ω for 55% moisture gluten dough at 25°C.

SIMULATION OF WHEAT FLOUR DOUGH RHEOLOGICAL PROPERTIES

Wheat doughs are highly viscoelastic materials and their rheology affects processing dramatically. For example, during sheeting, both steady shear and steady uniaxial extensional properties affect processing performance of the dough. The Bird–Carreau model is able to predict steady shear properties, but not the steady unaxial properties for which alternative constitutive models are considered (Wagner, 1976).

We conducted rheological measurements using an Instron Capillary Rheometer in the shear rate range of 2–1800 s^{-1}. Shear rate ranges from 10^{-4} to 10^{-1} s^{-1} were covered using a Rheometrics Mechanical Spectrometer (RMS-800). The Rheometrics constant stress rheometer was used to obtain viscosities at shear rates below 10^{-4} s^{-1}. Small amplitude oscillatory measurements were performed using the RMS and covered the range of 0.01–100 rad/s. Primary normal stress coefficient data for shear rates in the range of 9 to 60 s^{-1} were obtained using slit rheometry coupled with a Brabender extruder, shear stress and shear rates were calculated using the method of Han (1976).

Figure 16 shows the steady viscosity as a function of shear rate in the range of 10^{-6} to 10^{3}. The data obtained with three different methods are superimposable showing that the 40% moisture wheat flour tended towards a zero shear viscosity at shear rates below 10^{-5} s^{-1}. Data at such low shear rates have never been reported before. This material becomes non-Newtonian beyond the shear rate of 10^{-5} s^{-1} and does not appear to show significant structural transitions.

Figure 17 shows the primary normal stress coefficient ψ_1 as a function of shear rate in the shear rate

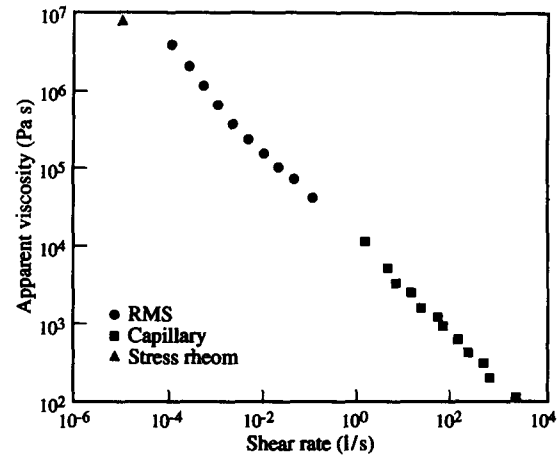

Fig. 16. Apparent viscosity (η) vs shear rate (γ) obtained using a mechanical spectrometer (RMS), a capillary rheometer, and a constant stress rheometer for 40% moisture wheat flour.

range of 10^{-4} to 10^{2} s^{-1}. Only data up to a shear rate of 5×10^{-2} s^{-1} could be obtained using the RMS and only data in the shear rate range of 5 to 80 s^{-1} could be obtained using slit rheometry during extrusion. However, the data appeared to follow power-law behavior. No zero shear trend was observed. To simulate the rheological properties of this 40% moisture hard wheat flour dough using the Bird–Carreau model, the following values for the empirical constants were used.

$\eta_0 = 8 \times 10^6$ Pa s; $\alpha_1 = 2.4942$; $\lambda_1 = 50\,000$ s;
$\alpha_2 = 1.8373$; $\lambda_2 = 3800$ s.

The experimental and predicted values of the steady viscosity function vs shear rate (Fig. 18) agree with each other. The nonlinear viscoelastic behavior of a wheat dough is of practical interest to scientists developing new products or technologies in the food industry. Because of the many different processing schemes in

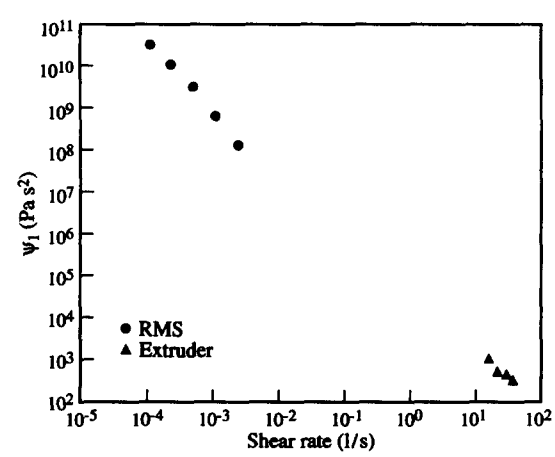

Fig. 17. Primary normal stress coefficient (ψ_1) vs shear rate (γ) using a mechanical spectrometer and slit die rheometry using a single extruder.

use, it is necessary to accurately predict the rheological behavior, especially the steady viscosity and the primary normal stress coefficient, throughout a shear rate range. The semi-empirical Bird–Carreau model is useful for this purpose.

PREDICTING CONCENTRATED APPLE PECTIN DISPERSIONS USING THE DOI–EDWARDS MODEL

To predict G' and G'' values for 5% pectin dispersion, the equations for a monodisperse as well as a polydisperse polymer were used (Shrimanker, 1989; Rahalkar *et al.*, 1985). For the polydisperse case, a computer program was developed to account for a small molecular fraction measured using low angle light scattering coupled with HPLC (Shrimanker, 1989). Figures 19 and 20 show the plot of predicted values of G' (ω) and G'' (ω), respectively, along with the experimental values. The polydisperse model fits the experimental data better than the monodisperse model. This is no surprise since apple pectin is highly polydisperse with ratios ($\overline{M_w}/M_n$) ranging from 15 to 45 (Chou & Kokini, 1987; Shrimanker, 1989). Although the simulations are quite good, especially with the modified equations, there is still a discrepancy between experimental and predicted values. It is difficult to pinpoint the reason or reasons at this stage, but many possibilities can be listed.

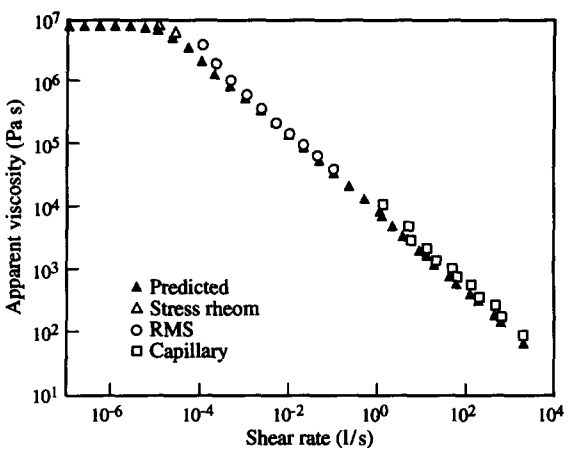

Fig. 18. Experimental values and those predicted using the Bird–Carreau model of the apparent viscosity (η) as a function of shear rate for hard flour dough sample.

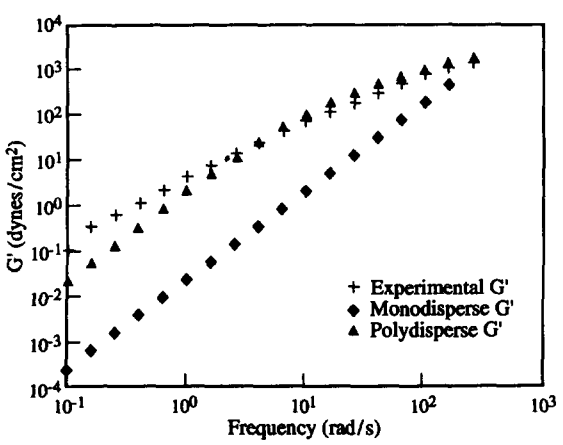

Fig. 19. G' values for 5% pectin solution predicted by the Doi–Edwards model.

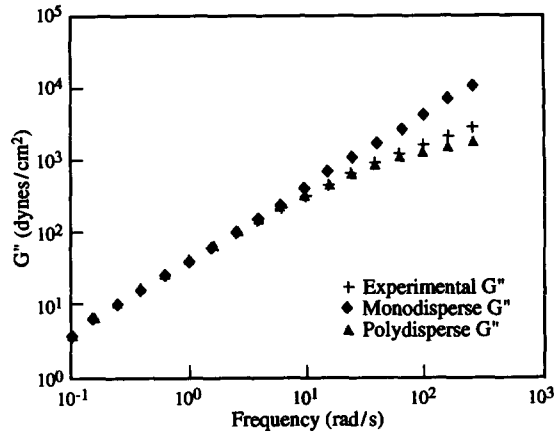

Fig. 20. G'' values for 5% pectin solution predicted by the Doi–Edwards model.

An inherent assumption of the theory is that the chains of different lengths can move only by reptation. However, the disengagement times of the longest chains may be much greater than the lifetime of the temporary cage. In that case, the longest chains may diffuse not only by reptation, but randomly directed segmental jumps. On the other hand, very short chains may diffuse laterally and not contribute to reptation.

Another factor which may influence reptation is branching. Apple pectins are constructed of homogalactouronan and rhamnogalactouronan regions with side chains of arabinogalactan. These side chains are highly branched (de Vries *et al.*, 1986). Short side branches (much shorter than the chain length between entanglement points) are expected to have a negligible effect upon reptation, while long and extensive branching may modify the characteristics of the cage and tube substantially.

Also, pectin is an anionic molecule, i.e. the chains are in more extended form as like charges repel each other. These extended, much longer chains can modify the characteristics of cage and tube considerably.

In apple pectin, which is a high molecular mass sample with broad molecular weight distribution, chains of all sizes are compelled to diffuse only by reptation, and yet the cage lifetimes, a communal property of the system may be very small compared to the disengagement time of the largest chains in the system.

CONCLUSION

Clearly there is need for much more work in this area of food rheology. It is first necessary to bring into the field constitutive models which can correctly predict extensional properties. Models for disperse system (suspensions, emulsions) rheology need to be developed. Progress has to be made in numerical methods so that non-linear constitutive models can be incorporated into process design. New models need to be designed which are capable of accounting for the diverse and complex structural properties of foods. Success in these efforts will result in better product design and process improvement rules leading to improved food products for the consumer.

ACKNOWLEDGEMENTS

This is paper D-10544-21-92 of the New Jersey Agricultural Experiment Station, supported by State Funds and the Center for Advanced Food Technology (CAFT) which is a New Jersey Commission on Science and Technology Center, National Science Foundation (NSF), the Campbell Soup Company and M & M Mars, a division of Mars Incorporated.

REFERENCES

Bagley, E.B. (1992). In *Food Extrusion Science and Technology*, Chap. 13. Marcel Dekker, Inc., New York, p. 203.

Bird, R.B., Armstrong, R.C. & Hassager, O. (1977). In *Dynamics of Polymeric Liquids*, Vol. 1. John Wiley and Sons, New York.

Bird, R.B., *et al.* (1987). In *Dynamics of Polymeric Liquids*, Vol. 1. John Wiley and Sons, New York.

Bistany, K.L. & Kokini, J.L. (1983). *J. Rheol.*, **27**, 605.

Chou, T.C. & Kokini, J.L. (1987). *J. Food Sci.*, **62**, 1658–64.

Cocero, A.M. & Kokini, J.L. (1991). *J. Rheol.*, **35**, 257–70.

Darby, R. (1976). In *Viscoelastic Fluids*. Marcel Dekker, Inc., New York.

de Vries, A.G., Voragen, J., Rombouts, F.M. & Pilnik, W. (1986). In *Chemistry and Function of Pectins*. American Chemical Society Symposium Series 310, Washington, DC, p. 38.

Doi & Edwards (1978*a*). *J. Chem. Soc., Part I, Faraday Trans. II*, **74**, 1789.

Doi & Edwards (1978*b*). *J. Chem. Soc., Part II, Faraday Trans. II*, **74**, 1802.

Doi & Edwards (1978*c*). *J. Chem. Soc., Part II, Faraday Trans. II*, **74**, 1818.

Dus, S.J. & Kokini, J.L. (1990). *J. Rheol.*, **34**, 1069–84.

Ferry, J.D. (1980). In *Viscoelastic Properties of Polymers*. John Wiley and Sons, Inc., New York.

Glicksman, M. (1982). In *Food Hydrocolloids*, ed. A. Glicksman, Vol. 1. CRC Press, Boca Raton, Florida, p. 4.

Gordon, M. & Taylor, J.S. (1952). *J. Appl. Chem.*, **2**, 493–500.

Han, C.D. (1976). In *Rheology in Polymer Processing*. Academic Press, New York.

Hoseney, R.C., Zeleznak, K. & Lai, C.S. (1986). *Cereal Chem.*, **63**, 285–6.

James, H.M. (1947). *J. Chem. Phys.*, **15**, 651.

Kokini, J.L., Bistany, K. & Mills, P. (1984). *J. Food Sci.*, **49**, 1569.

Kokini, J.L. & Plutchok, G.J. (1987). *Food Technol.*, **41**, 89–95.

Leppard, W.R. (1975). Viscoelasticity: stress measurements and constitutive theory. PhD Thesis, University of Utah.

Marvin, R.S. & McKinney, J.E. (1965). In *Physical Accoustics*, ed. W.P. Mason, Vol. B. Academic Press, New York.

Plutchok, G. & Kokini, J.L. (1986). *J. Food Sci.*, **51**, 1284.

Rahalkar *et al.* (1985). *J. Rheol.*, **29**, 955–70.

Rouse, Jr, P.E. (1953). *J. Chem. Phys.*, **21**, 1272.

Schurz, J. (1976). *Proc. 7th Int. Congr. on Rheology*, Chalmus University of Technology, Gothenburg, Sweden, eds C. Klason & J. Kubat, p. 123.

Shrimanker, S.H. (1989). Evaluation of the Doi–Edwards theory for predicting viscoelastic properties of food biopolymers. MS Thesis, Rutgers University.

Wagner, M.H. (1976). *Rheol. Acta*, **15**, 136–42.

Williams, M.L., Landel, R.F. & Ferry, J.D. (1955). *J. Am. Chem. Soc.*, **77**, 3701–6.

Zimm, B.H. (1956). *J. Chem. Phys.*, **24**, 269.